Available online at www.sciencedirect.com
ScienceDirect
Journal of Power Sources 172 (2007) 913–918
JOURNAL OF POWER SOURCES
www.elsevier.com/locate/jpowsour

Short communication

# Synthesis and electrochemical characterization of carbon-coated nanocrystalline $LiFePO_4$ prepared by polyacrylates-pyrolysis route

Y.L. Cao, L.H. Yu, T. Li, X.P. Ai, H.X. Yang *

*Department of Chemistry, Wuhan University, Wuhan 430072, PR China*

Received 21 September 2006; received in revised form 4 May 2007; accepted 9 May 2007
Available online 18 May 2007

**Abstract**

A carbon-coated nanocrystalline $LiFePO_4$ cathode material was synthesized by pyrolysis of polyacrylate precursor containing $Li^+$, $Fe^{3+}$ and $PO_4^-$. The powder X-ray diffraction (XRD) and high-resolution TEM micrographs revealed that the $LiFePO_4$/C composite as prepared has a core-shell structure with pure olivine $LiFePO_4$ crystallites as cores and intimate carbon coating as a shell layer. Between the composite particulates, there exists a carbon matrix binding the nanocrystallites together into micrometer particles. The electrochemical measurements demonstrated that the $LiFePO_4$/C composite with an appropriate carbon content can deliver a very high discharge capacity of 157 mAh $g^{-1}$ (>92% of the theoretical capacity of $LiFePO_4$) with 95% of its initial capacity after 30 cycles. Since this preparation method uses less costly materials and operates in mild synthetic conditions, it may provide a feasible way for industrial production of the $LiFePO_4$/C cathode materials for the lithium-ion batteries.


*Keywords:* $LiFePO_4$/C composite; Cathode material; Li-ion batteries; Polyacrylates-pyrolysis

## 1. Introduction

Olivine $LiFePO_4$ is now considered to be a promising cathode material for large capacity Li-ion batteries because of its low cost of starting materials, excellent reversibility and thermal stability [1–7]. However, there are two basic problems hindering the practical application of this material for high rate Li-ion batteries. One is the poor electronic and ionic conduction in the crystalline lattice of $LiFePO_4$, in which large $PO_4^{3-}$ polyanions separate the chains of edge-shared $FeO_6$ octahedra. To solve this problem, much effort has been made by coating conductive carbon or metals on the $LiFePO_4$ surface [8–18] or by doping super-valence ions in the crystalline lattice [19–21]. It have been reported the $LiFePO_4$ sample containing 3.5 wt.% coated-carbon can reach a discharge capacity of 160 mAh $g^{-1}$, which is very close to its theoretical capacity of 170 mAh $g^{-1}$ [11].

Another problem for industrial production of $LiFePO_4$ material is the difficulty to obtain a pure-phase $LiFePO_4$ compound because $Fe^{2+}$ is easy to be oxidized to $Fe^{3+}$ during the course of synthesis, leading to the formation of impure phases aside from olivine phase. In the solid-state synthesis of $LiFePO_4$, the reaction condition, such as atmosphere and temperature, needs to be strictly controlled to prevent the oxidation of iron ions, and also the raw materials of iron need to be pure divalent iron compounds. These requirements bring about a considerable increase in the costs of materials and production.

In previous studies, there are mainly two methods reported for preparation of the $LiFePO_4$ composites. The mostly used one was the solid-state ceramic method [22,23] and the other was a sol–gel method [24,25]. Both of the synthetic methods can give the resulting composites with homogeneous crystallites and good electrochemical performances. However, the former method is very time-consuming and easy to produce large-size particles with impure phases due to inhomogeneous mixing of raw materials. Although the sol–gel method can produce uniformly sized $LiFePO_4$ crystallites with homogeneous distribution of metallic ions, it involves complicated pretreatment processes, which are difficult to control for industrial application. Thus, it is of practical importance to seek a feasible method for preparation of $LiFePO_4$ with low cost raw material and easily controllable synthetic conditions.

* Corresponding author. Tel.: +86 27 68754526; fax: +86 27 87884476.
*E-mail address:* ece@whu.edu.cn (H.X. Yang).

0378-7753/$ – see front matter © 2007 Published by Elsevier B.V.
doi:10.1016/j.jpowsour.2007.05.013

In this work, we report a novel and simple method for synthesis of nanocrystalline $LiFePO_4$/C composites by pyrolyzing the $Li^+$–$Fe^{3+}$–$PO_4^{3-}$ polyacrylates, which are prepared as precursors via in situ polymerization of $Li^+$, $Fe^{3+}$ and $PO_4^{3-}$ acrylates, and also we describe the structural and electrochemical characteristics of the $LiFePO_4$/C composites.

## 2. Experimental

The polymeric precursor was prepared by dissolving the stoichiometric LiOH, $Fe(NO_3)_3{\cdot}9H_2O$ and $NH_4H_2PO_4$ (1:1:1, molar ratio) in aqueous acrylic acid solution at continuous stirring and then polymerizing the mixed acrylic acid solution using a small amount of $(NH_4)_2S_2O_8$ aqueous solution as an initiator. In order to make a comparison, three samples with different ratios of Li to acrylic acid (1:4, 1:2 and 1:1) were prepared and marked as S14, S12 and S11. Under heating at ~80 °C for 2 h, the mixed solution was polymerized to the well-distributed polyacrylates of $Li^+$, $Fe^{3+}$ and $PO_4^{3+}$. Then the polymeric precursor was dried at 120 °C for 12 h. The dried copolymeric precursor in a crucible was buried in active carbon and pyrolyzed at 600 °C for 5 h. During the decomposition process of the polymeric precursor, the trivalent Fe was reduced to bivalent Fe. In order to improve the formation of $LiFePO_4$, the pyrolyzed powders were then sintered in the tube furnace in Ar atmosphere at 800 °C for 5 h to obtain the final samples of $LiFePO_4$ composite. For comparison, the sample with the ratio of Li to acrylic acid (1:2) pyrolyzed at 600 °C was marked as S12-600.

The carbon contents in the $LiFePO_4$ samples were revealed by thermogravimetric and differential thermal analysis (TG/DTA) on a model WCT-1A thermobalance (Beijing Optical Instrument Factory) at a temperature range of 30–950 °C with a heating rate of 10 °C $min^{-1}$ in oxygen. In order to demonstrate the crystalline structure of the $LiFePO_4$ powders, X-ray diffraction (XRD) and high-resolution transmission electron microscopy (HRTEM) were carried out on a Shimadzu XRD-6000 diffractometer with Cu Kα and on a JEM-2010FEF TEM system, respectively.

The cathode used in this work with a geometrical area of 2 $cm^2$ consisted of 80% $LiFePO_4$ powders, 12% acetylene black and 8% poly(tetrafluoroethylene) (PTFE) by weight. The electrode was prepared by mixing the $LiFePO_4$ powders, acetylene black and PTFE emulsion with 2-propanol to form an electrode paste, then rolling the paste into a ca. 0.1-mm-thick film, and finally pressing the electrode film onto an aluminum foil.

The galvanostatic charge–discharge measurements were performed in a three-electrode cell of a sandwiched design. $LiFePO_4$ electrode and lithium electrode were separated by a microporous membrane (Celgard 2400) and pressed in parallel together by a pair of electrode holders. A small piece of lithium foil immersed in the electrolyte served as a reference electrode. The electrolyte was 1 mol $L^{-1}$ $LiPF_6$ dissolved in a mixed solution of ethylene carbonate (EC)-dimethyl carbonate (DMC)-ethylene methyl carbonate (EMC) (1:1:1, w/w/w). All the cells were assembled in a dry box filled with argon gas. The galvanostatic charge–discharge test was conducted by a BTS-55 Neware battery testing system at various rates (1 C = 157 mA $g^{-1}$, $LiFePO_4$).

## 3. Results and discussion

In previous papers, we demonstrated the feasibility of the polyacrylate-pyrolysis method (PPM) for preparation of nanocrystalline Li–Ni–Mn–O materials using copolymerized acrylates of $Li^+$, $Mn^{4+}$ and $Ni^{2+}$ as polymer precursors [26,27]. For preparing the $LiFePO_4$/C composite, we firstly prepared the copolymer precursor containing $Li^+$, $Fe^{3+}$ and $PO_4^{3-}$ sim-

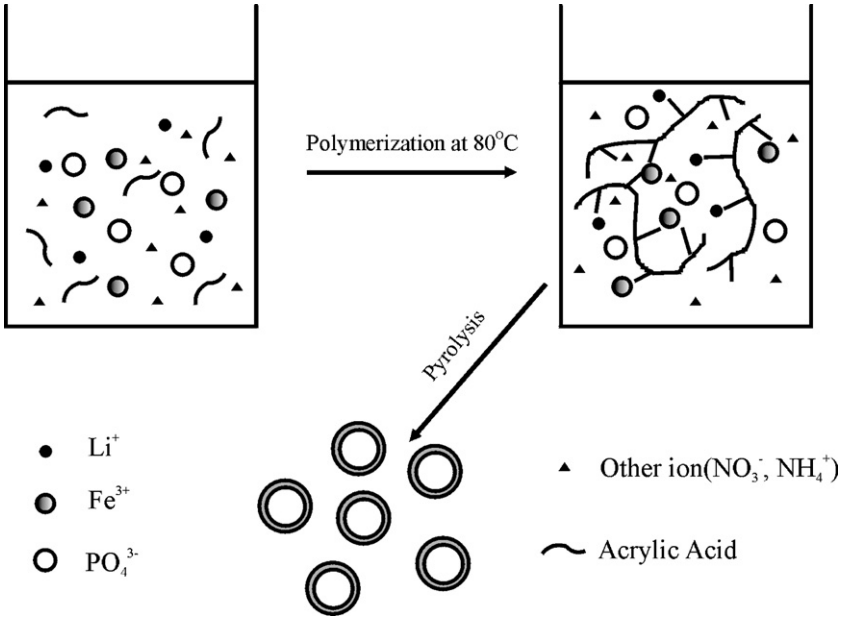


Fig. 1. A schematic diagram of the PPM process for preparation of $LiFePO_4$/C composite.

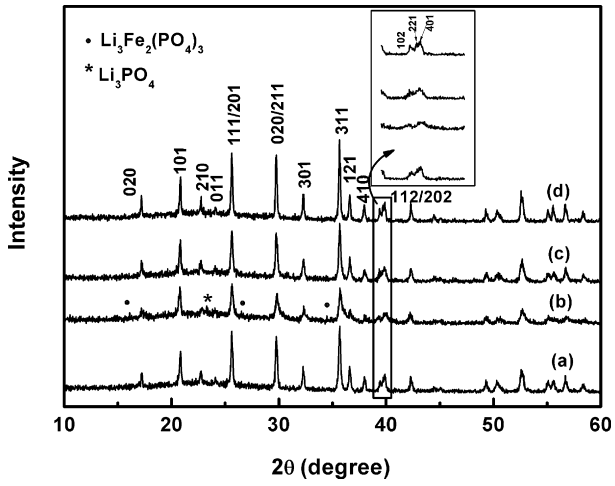


Fig. 2. The XRD patterns of the $LiFePO_4$/C samples: (a) S11, (b) S12-600 (S12 heat-treated at 600 °C only), (c) S12 and (d) S14.

ply by dissolving a stoichiometric amount of LiOH, $Fe(NO_3)_3$ and $NH_4H_2PO_4$ in aqueous acrylic acid (AA) solution and then pyrolyzed the copolymer at reductive atmosphere to form the $LiFePO_4$/C composite material. A schematic representation of the synthetic process is shown in Fig. 1.

In this synthetic process, the initial polymerizable AA concentration and subsequent pyrolysis temperature are the two important factors determining the structural and electrochemical performances of the $LiFePO_4$/C composites. In general, an increase in the pyrolytic temperature can increase the crystallinity and size of $LiFePO_4$ particles, which can increase the electrochemical capacity but decrease the rate capability of the material. Higher concentration of AA monomer in the solution would result in higher carbon content in the $LiFePO_4$/C composite, which helps to enhance the electronic conductivity but lowers the tapping density and specific capacity of the material. In order to obtain the $LiFePO_4$/C composite with appropriate crystalline size and carbon content, we optimized the chemical compositions of the copolymer precursors and pyrolytic temperature for synthetic reaction of $LiFePO_4$/C composite.

Fig. 2 shows the XRD patterns of the $LiFePO_4$ samples pyrolyzed from the different copolymeric precursors and calcined at 600 and 800 °C, respectively. Compared with the published XRD data of Li–Fe–P–O compounds (81-1173# in JCPDS database), all the samples can be assigned to olivine $LiFePO_4$ with orthorhombic lattice (*Pnma*) and almost no impurity phases are detected except for the sample calcined only at 600 °C (Fig. 2b). Some weak XRD signals reflecting $Li_3PO_4$ and $Li_3Fe_2(PO_4)_3$ phases only appeared in the sample at the pyrolytic temperature of 600 °C, indicating incomplete reduction of $Fe^{3+}$ to $Fe^{2+}$ at low temperature treatment. Once the samples were further sintered at 800 °C in Ar, all the XRD lines due to the impurities disappeared and the XRD peaks of $LiFePO_4$ become sharper and stronger, demonstrating that the $LiFePO_4$ samples were very well-crystallized at 800 °C. This explanation is also supported by the appearance of three splitting peaks at $2\theta = 39$–$41°$ for the samples sintered at 800 °C as shown in the inset in Fig. 2, which represents the crystalline integrity of $LiFePO_4$. The broad hills at $2\theta = 20$–$25°$ shown in Fig. 2 in all the samples indicate the existence of amorphous crystalline structures of carbon, which were formed by the pyrolysis of polyacrylate.

The lattice parameters of all the samples calculated from the XRD patterns based on the *Pnma* space group are summarized in Table 1. As it is shown, the lattice parameters are increased with an increase in sintering temperature, similarly as reported by Cho and Chung [28]. This phenomenon is probably due to a change in the ionic radius of iron from a smaller value of trivalent iron ($Fe^{3+}$, 0.645 Å) to a larger value of divalent iron ($Fe^{2+}$, 0.770 Å), because the trivalent iron tends to be reduced to the divalent one at reductive atmosphere and increased temperature. Another phenomenon as shown in Table 1 is that the calculated lattice parameters decrease with increasing carbon content in the final products such as for the samples S11, S12 and S14. The variation in the lattice parameters with the carbon content can be attributed to a change in the crystallinity of the samples, which is greatly altered by the amount of coated carbon.

Fig. 3 shows the TEM image of the sample S12 pyrolyzed at 600 °C in air-deficient atmosphere and then sintered at 800 °C in Ar. As shown in Fig. 3a, the $LiFePO_4$ particles have sphere-like shape with particle size of ~50 nm dispersed in the matrix carbon. The residual carbon pyrolyzed from the polyacrylate forms a matrix structure to binder the $LiFePO_4$ particles together and to provide a good electric connection between the particles. Also, the carbon matrix provides a hindrance for the aggregation and growth of the particles [24,29,30]. Fig. 3b shows the high-resolution TEM (HRTEM) image of a $LiFePO_4$ particle. As shown in this image, three different zones are clearly distinguishable, reflecting three types of the crystalline structures. In the inner part of a particle, the HRTEM shows a regular parallel pattern and correspondingly the selected-area diffraction (SAD) spectrum (higher right inset in Fig. 3b) gives a well-defined diffraction pattern of olivine phase, suggesting a well-crystallized $LiFePO_4$ phase formed as the core of the particle. On the surface of the $LiFePO_4$ crystallites, there is

Table 1
Lattice parameter and electrochemical properties of the $LiFePO_4$/C samples synthesized at different PPM conditions

| | Pyrolytic temperature (°C) | AA: $LiFePO_4$ | Lattice parameters | | | | Carbon content (wt.%) | Initial discharge capacity (mAh $g^{-1}$) |
|---|---|---|---|---|---|---|---|---|
| | | | *a* (Å) | *b* (Å) | *c* (Å) | V | | |
| S11 | 600/800 | 1 | 10.3135 | 6.0121 | 4.7034 | 291.638 | 3.5 | 105 |
| S12-600 | 600 | 2 | 10.2944 | 6.0042 | 4.6951 | 290.202 | – | 94 |
| S12 | 600/800 | 2 | 10.3054 | 6.0116 | 4.7031 | 291.369 | 10.4 | 157 |
| S14 | 600/800 | 4 | 10.3050 | 6.0115 | 4.6998 | 291.145 | 24.4 | 100 |

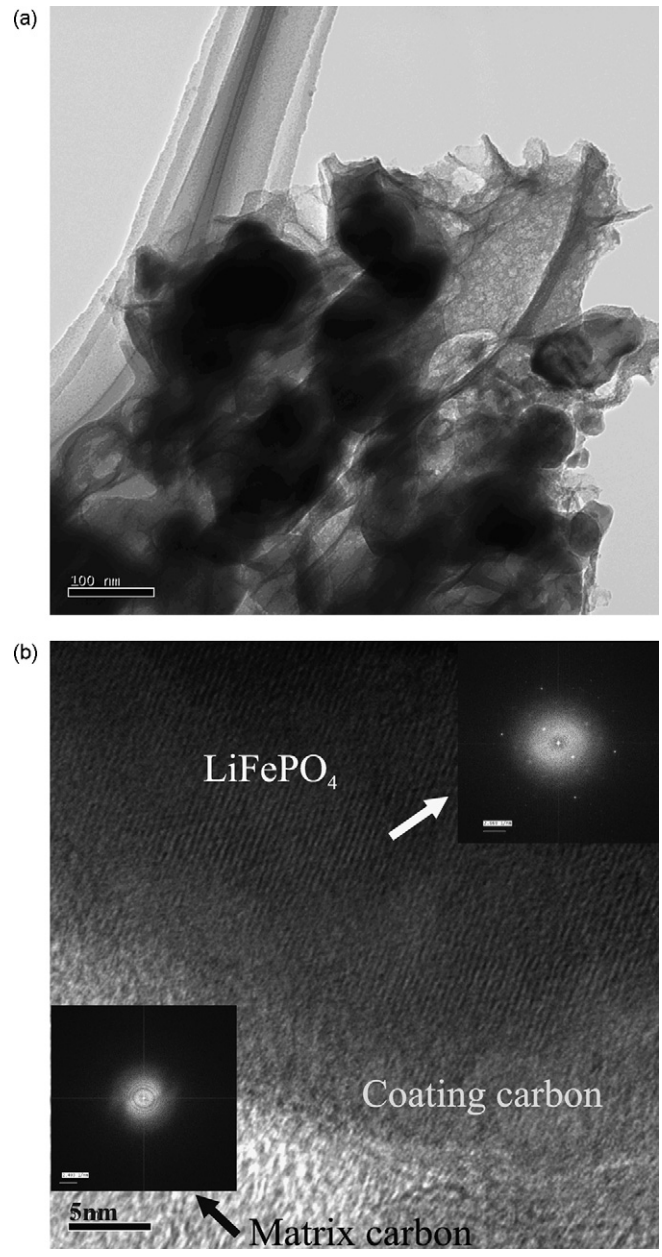


Fig. 3. (a) The TEM image of the $LiFePO_4$/C sample: S12 and (b) the HR-TEM image of a selected particle in Fig. 3a.

a dense layer of amorphous structure with several nanometers thick, probably due to the intimately coated carbon. In-between the particles, there exists a binding matrix, representing the amorphous phase of loosely bounded carbon as shown by the diffraction hollow ring in the SAD pattern (lower left inset in Fig. 3b). These results demonstrate that the $LiFePO_4$/C composite synthesized from the PPM method has a perfect crystalline $LiFePO_4$ phase, uniform size distribution and intimate carbon coating.

To determine the carbon content in the $LiFePO_4$/C samples, we used TG and DTA methods to measure the amount of carbon released from the samples during the temperature scan in oxygen atmosphere. In the TG curve of sample S14 (Fig. 4a), there are two weight-losing processes appearing at 330–480 °C and 480–560 °C with a total weight loss of 20.5%, including the weight loss due to the carbon oxidation and the weight gain due to the $Fe^{2+}$ oxidation in the $LiFePO_4$/C sample. Considering that the matrix carbon is well-dispersed fine carbon particles and easily ignitable than the densely coated carbon layer, the two steps of weight losses at 330–480 °C and at 480–560 °C are most likely due to the oxidations of the matrix carbon and the coated carbon, respectively. In accord with the TG data, there are two exothermic peaks appearing at the temperature regions in the

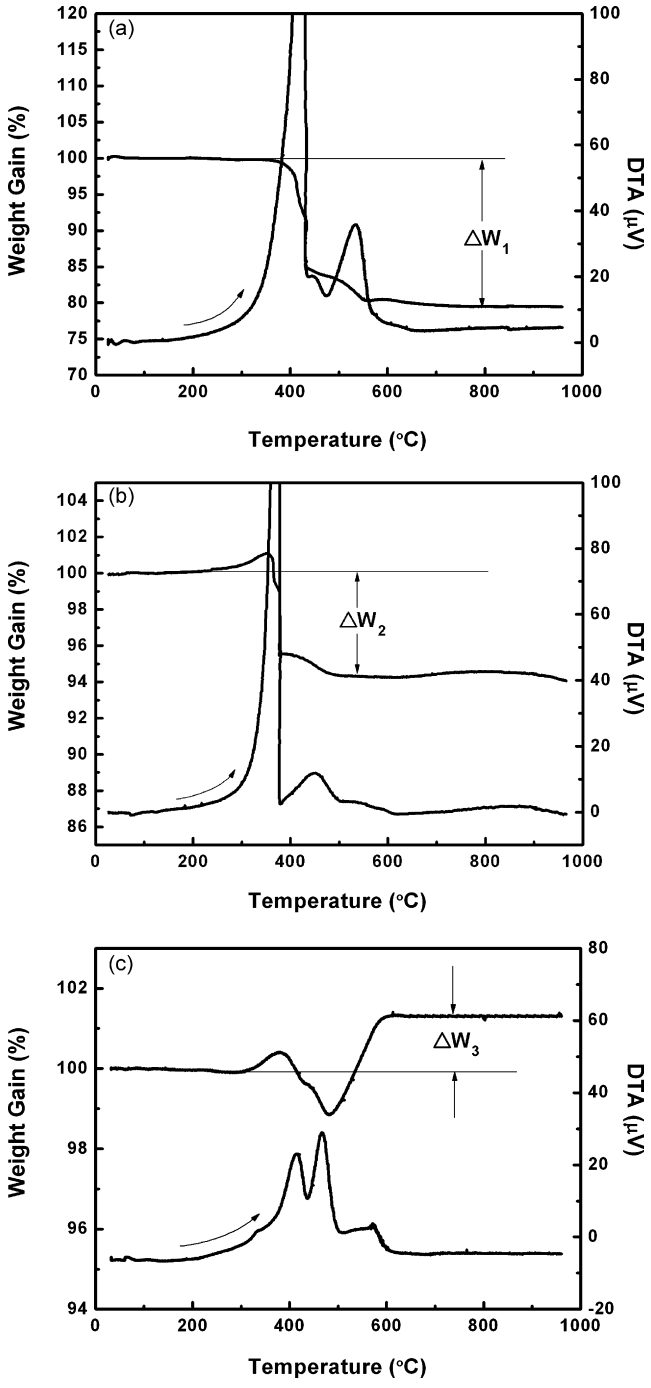


Fig. 4. (a) The TG curve of the sample S14 tested in oxygen, (b) the TG curve of the sample S12 tested in oxygen and (c) the TG curve of the sample S11 tested in oxygen.

DTA curve correspondingly, indicating the stepwise oxidation of the carbon in the samples. It should be mentioned that in the temperature range of 230–530 °C, the oxidation of $Fe^{2+}$ ions must also be taken place in the way as follows [6]:

$$LiFePO_4 + \tfrac{1}{4}O_2 \rightarrow \tfrac{1}{3}Li_3Fe_2(PO_4)_3 + \tfrac{1}{6}Fe_2O_3 \quad (1)$$

According to this reaction scheme, the theoretical weight gain of 5.07% for the $LiFePO_4$ samples should be observed and must be taken into account in calculation of the carbon content from the TG data. Since the weight gain in the oxidation of $LiFePO_4$ is much less than the weight loss in the carbon oxidation, the TG and DTA features for the oxidation of $LiFePO_4$ all appear as a small shoulder at 380–450 °C in the TG and DTA curves, which are heavily screened by the strong exothermic oxidation bands of carbon. According to the well-accepted method for calibration of the carbon content in the $LiFePO_4$/C composite [13], the actual amount of carbon can be calculated from the weight loss of the sample measured from the TG curve plus the 5.07% weight gain due to the $Fe^{2+}$ oxidation, and therefore, the carbon content for the sample S14 is calculated to be about 24.4%.

Analogously, the sample S12 and S11 exhibit very similar TG and DTA behaviors as shown in Fig. 4b and c, except for the changes in the relative intensities of the three exothermic bands. In these figures, both the weight losses and DTA intensities of the matrix carbon and the coated carbon decrease with lowering the acrylic content in the samples, while the DTA peak due to the oxidation of $LiFePO_4$ becomes evident. The carbon contents calculated for the sample S12 and S11 are 10.4 and 3.5%, demonstrating that the carbon content in the samples can be controlled by adjusting the acrylic monomer concentration in preparation of copolymer precursor.

Fig. 5 shows the typical charge–discharge curves of the Li-$LiFePO_4$/C cells cycled between 2.5 and 4.0 V at a current density of 0.15 C. It can be seen that except for the sample S12-600 (Fig. 5b), All other $LiFePO_4$/C electrodes showed a single charge–discharge plateau around 3.45 V versus $Li/Li^+$, suggesting a simple lithium intercalation–deintercalation reaction in pure olive $LiFePO_4$ phase, as reported previously by Padhi et al. [1]. The appearance of lower voltage plateau at 2.6 V for the sample S12-600 suggests the existence of impure phase, probably $Li_3Fe_2(PO_4)_3$, in the sample, which is caused by the incomplete reduction of $Fe^{+3}$ ions at 600 °C as indicated in the XRD evidence in Fig. 2. Among the $LiFePO_4$/C composites tested, the sample S12 (Fig. 5c) with 10.4 wt.% carbon content and heat-treated at 800 °C exhibited highest discharge capacity of 157 mAh $g^{-1}$, about 92% of the theoretical capacity of $LiFePO_4$. It should be noticed that the carbon content can affect the electrochemical capacity of the materials dramatically, and higher content of coated carbon also results in a rapid decrease in the charge–discharge capacity of the composite material. This phenomenon could be explained that at lower carbon content, the electrochemical capacity of the $LiFePO_4$ could not be fully utilized due to the lower conductivity and larger particle size of the material such as in the case of the sample S11 (Fig. 5a). When the carbon is over-loaded, a thick layer of dense carbon coating must be formed on the surfaces of the $LiFePO_4$ particles, which can block the transfer of lithium ions from electrolyte solution into the $LiFePO_4$ particle, as in the case of sample S14 (Fig. 5d). It seems that an appropriate carbon coating play a key role in determining the capacity utilization of the $LiFePO_4$/C composite, which should enhance not only the electronic conduction but also the ionic diffusion in the particles.

The rate capability of the sample S12 is shown in Fig. 6. Like all the inserting electrode materials, the discharge capacity of the $LiFePO_4$/C composite decreases with increasing current density, showing a diffusion-limited transfer of lithium ions across the surface and in the interior lattice of the $LiFePO_4$ particles. However, at moderate rate of charge and discharge, the $LiFePO_4$ electrode can still release a discharge capacity of 137 mAh $g^{-1}$, ca. 82% of theoretical capacity (168 mAh $g^{-1}$). When the current density is increased to a high rate of 1 C, the discharge capacity of the electrode reduces to 110 mAh $g^{-1}$, showing a certain capability for high rate charge and discharge.

Fig. 7 shows the capacity retention of the $LiFePO_4$ samples versus cycling number. As shown in the figure, the cycling stability of these materials is very different, apparently depending on the carbon content of the composite materials. For the

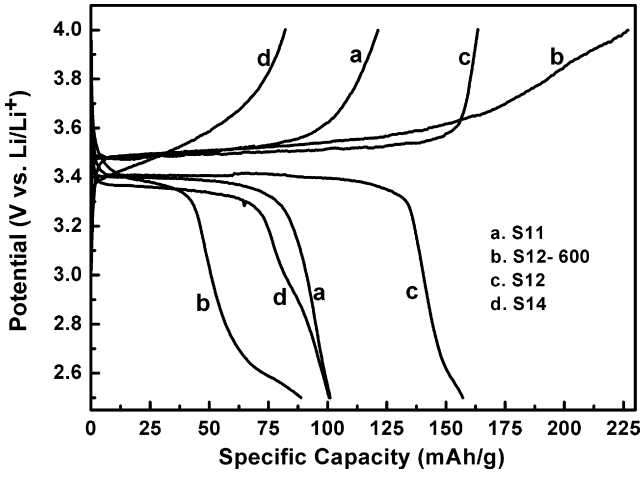


Fig. 5. The charge–discharge curves of the $LiFePO_4$/C electrodes obtained at different synthetic conditions at 0.15 C rate.

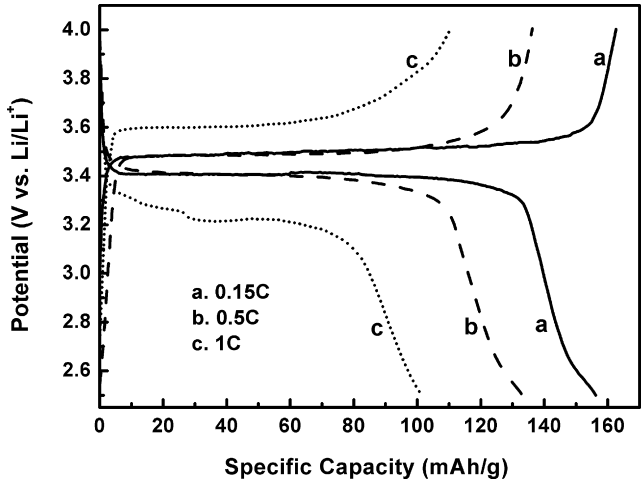


Fig. 6. The charge–discharge curves of the S12 electrode at (a) 0.15, (b) 0.5 and (c) 1 C rate.

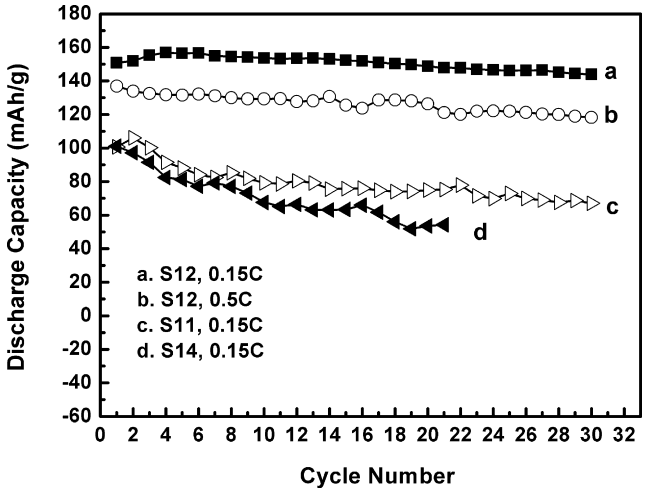


Fig. 7. The capacity retention of the $LiFePO_4$/C samples cycled at 2.5–4.0 V.

sample S11 with low carbon content (Fig. 7d), the discharge capacity decreases rapidly from initial 110 to 60 mAh $g^{-1}$ at 20th cycle, showing a poorest cycling performance in the samples tested. This phenomenon may be explained according to a stress change as suggested by Wang et al. [31] which attributed the capacity fading of the $LiFePO_4$/C composite to the formation of cracks and subsequent pulverization of the material due to the volumetric change of the $LiFePO_4$ crystals during $Li^+$ insertion/de-insertion cycling. For the sample S14 with high carbon content (Fig. 7c), the cycling capacity drops mainly in first ten cycles and then remains quite stable after prolonged cycling. This improved cycling stability for the sample with higher carbon content is possibly due to the buffering effect of the coated carbon layer, which buffers the volumetric change of $LiFePO_4$ during cycling. As expected, the sample with appropriate carbon coating exhibits excellent cycling ability with very slight capacity degradation during charge–discharge cycling.

## 4. Conclusions

This paper describes a novel route for preparing highly homogeneous nanocrystalline $LiFePO_4$/C powders by the pyrolysis of a copolymeric precursor containing polyacrylates of $Li^+$ and $Fe^{3+}$ and phosphate. The data from the XRD and TEM measurements revealed that the $LiFePO_4$/C powders are composed of nanosized $LiFePO_4$ crystallites with carbon-coated shells and a carbon matrix binding the composite particles together into sphere-like particles. It has been found that the electrochemical performances of the $LiFePO_4$/C composite depend greatly on the carbon content in the composite material. The $LiFePO_4$/C sample with appropriate carbon content can deliver a very high discharge capacity of 157 mAh $g^{-1}$ (>92% of the theoretical capacity of $LiFePO_4$) with 95% of its initial capacity after 30 cycles. Also, the as-prepared $LiFePO_4$/C electrode can exhibit a quite good high rate capability of 110 mAh $g^{-1}$ at 1 C rate.

In addition, this new preparation method uses inexpensive starting materials and operates in mild synthetic conditions, and therefore, it may provide a feasible way for industrial production of the $LiFePO_4$/C cathode materials for the lithium-ion batteries.

## Acknowledgements

We acknowledge financial support by the 973 Program, China (grant 2002CB211800) and the National Science Foundation of China (no. 50502025).

## References

[1] A.K. Padhi, K.S. Nanjundaswamy, J.B. Goodenough, J. Electrochem. Soc. 144 (1997) 1188–1194.
[2] A.K. Padhi, K.S. Nanjundaswamy, C. Masquelier, S. Okada, J.B. Goodenough, J. Electrochem. Soc. 144 (1997) 1609–1613.
[3] A. Yamada, S.C. Chung, K. Hinokuma, J. Electrochem. Soc. 148 (2001) A224–A229.
[4] A. Deb, U. Bergmann, E.J. Cairns, S.P. Cramer, J. Phys. Chem. B 108 (2004) 7046–7051.
[5] N. Iltchev, Y. Chen, S. Okada, J. Yamaki, J. Power Sources 119–121 (2003) 749–754.
[6] I. Belharouak, C. Johnson, K. Amine, Electrochem. Commun. 7 (2005) 983–988.
[7] S. Zhu, H. Zhou, T. Miyoshi, M. Hibino, I. Honma, M. Ichihara, Adv. Mater. 16 (2004) 2012–2017.
[8] H. Huang, S. Yin, L.F. Nazar, Electrochem. Solid-State Lett. 4 (2001) 170.
[9] S. Franger, F. Cras, C. Bourbon, H. Rouault, Electrochem. Solid-State Lett. 5 (2002) 231.
[10] G. Li, H. Azuma, M. Tohda, J. Electrochem. Soc. 149 (2002) 743.
[11] Zh. Chen, J.R. Dahn, J. Electrochem. Soc. 149 (2002) 1184.
[12] N. Ravet, Y. Chouinard, J. Magnan, F.S. Besner, M. Gauthier, M. Armand, J. Power Sources 97/98 (2001) 503.
[13] S. Yang, Y. Song, P. Zavalij, M. Whittingham, Electrochem. Commun. 4 (2002) 239.
[14] F. Croce, A. D'Epifanio, J. Hassoun, A. Deptula, T. Olczac, B. Scrosati, Electrochem. Solid-State Lett. 5 (2002) 47.
[15] J. Barker, M.Y. Saidi, J.L. Swoyer, Electrochem. Solid-State Lett. 6 (2003) 53.
[16] M.M. Doeff, Y. Hu, Q.F. McLarnon, R. Kostecki, Electrochem. Solid-State Lett. 6 (2003) 207.
[17] M. Herstedt, M. Stjerndahl, A. Nytén, T. Gustafsson, H. Rensmo, H. Siegbahn, N. Ravet, M. Armand, J.O. Thomas, K. Edström, Eletrochem. Solid-State Lett. 6 (2003) 202.
[18] S. Myung, S. Komaba, R. Takagai, N. Kumagai, Y. Lee, Chem. Lett. 7 (2003) 566.
[19] S. Chung, J. Bloking, Y. Chiang, Nat. Mater. 2 (2002) 123.
[20] G.X. Wang, S.L. Bewlay, J. Yao, J.H. Ahn, S.X. Dou, H.K. Liu, Electrochem. Solid-State Lett. 7 (12) (2004) A503–A506.
[21] G.X. Wang, S.L. Bewlay, K. Konstantinov, H.K. Liu, S.X. Dou, J.H. Ahn, Electrochim. Acta 50 (2004) 443–447.
[22] P.P. Prosini, D. Zane, M. Pasquli, Electrochim. Acta 46 (2001) 3517.
[23] A.S. Andersson, J.O. Thomas, J. Power Sources 97–98 (2001) 498.
[24] K.F. Hsu, S.Y. Tsay, B.J. Hwang, J. Mater. Chem. 14 (2004) 2690–2695.
[25] Y.Q. Hu, M.M. Doeff, R. Kostecki, R. Finones, J. Electrochem. Soc. 151 (2004) A1279.
[26] L.H. Yu, H.X. Yang, X.P. Ai, Y.L. Cao, J. Phys. Chem. B 109 (2005) 1148–1154.
[27] L.H. Yu, Y.L. Cao, H.X. Yang, X.P. Ai, J. Solid State Electrochem. 10 (2006) 283–287.
[28] T.H. Cho, H.T. Chung, J. Power Sources 133 (2004) 272–276.
[29] C.H. Mi, X.B. Zhao, G.S. Cao, J.P. Tu, J. Electrochem. Soc. 152 (2005) A483–A484.
[30] S.T. Myung, S. Komaba, N. Hirosaki, H. Yashiro, N. Kumagai, Electrochim. Acta 49 (2004) 4213–4222.
[31] D. Wang, X.D. Wu, Z.X. Wang, L.Q. Chen, J. Power Sources 140 (2005) 125–128.